ACS APPLIED NANO MATERIALS

www.acsanm.org Article

Three-Dimensional Nanoporous Covalent Organic Framework-Incorporated Monolithic Columns for High-Performance Liquid Chromatography

Xue Liu, Cheng Yang, Hai-Long Qian,* and Xiu-Ping Yan*

Cite This: *ACS Appl. Nano Mater.* 2021, 4, 5437−5443 Read Online

ACCESS | Metrics & More | Article Recommendations | Supporting Information

ABSTRACT: The application of three-dimensional covalent organic frameworks (3D COF) with complex structure and high stability as the stationary phase is promising for high-performance liquid chromatography (HPLC) but is still limited by their irregular shape and wide size distribution. Herein, we show the fabrication of the first 3D COF-based monolithic column via the facile incorporation of nanoporous 3D-IL-COF-1 consisting of tetrakis(4-formylphenyl)methane and *p*-phenylenediamine into a porous organic monolith for HPLC. The effect of essential factors including temperature, porogen, and 3D-IL-COF-1 on the column permeability and efficiency is systematically investigated via the orthogonal experiment. The uniform structure, good permeability, and high mechanical stability of the prepared 3D-IL-COF-1 monolithic column not only make it promising for broad-spectrum chromatographic separation of neutral, acidic, and basic compounds but also render it better separation of isomers than a C18 column. This work offers a facile strategy for synthesis of a 3D COF stationary phase and will largely expand the high potential of 3D COF in HPLC.

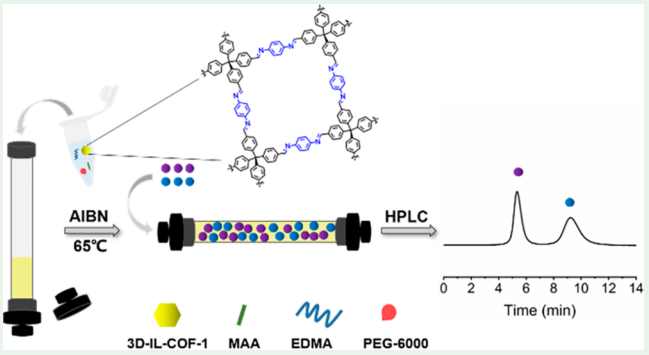

KEYWORDS: *three-dimensional covalent organic frameworks, stationary phase, monolithic column, high-performance liquid chromatography, isomer*

INTRODUCTION

Covalent organic frameworks (COF) are porous crystalline materials consisting of organic monomers[1,2] and show wide applications in chemistry and environmental and biomedical sciences.[3−9] The separation properties of high-performance liquid chromatography (HPLC) are mainly attributed to the noncovalent interactions between analytes and the stationary phase including hydrophobic, hydrophilic, electron donor−acceptor interaction, size exclusion, and even hand-specific interaction.[10,11] The discovery of new versatile materials as the stationary phase with distinctive interactions is of great significance in the improvement of chromatographic separation. The large surface area, great stability, and tunable pore chemistry of COF with rich interactions such as $\pi-\pi$, hydrophobic, and hydrogen-bonding interactions give them potential as the stationary phase of HPLC.[12]

Three-dimensional (3D) COF are completely linked with covalent bonds. As a result, 3D COF exhibit higher stability and richer pore structures than 2D COF formed via covalent bands and $\pi-\pi$ stacking interactions.[1,13,14] 2D COF have shown great potential to be the stationary phase of both liquid and gas chromatography,[15−18] whereas exploration of 3D COF for chromatography is still in its infancy.[19] Exploring the potential of 3D COF in the field of HPLC separation is of great significance for promoting the materials in separation science.

The direct application of bulky 3D COF as the stationary phase suffers from a high column pressure and low column efficiency owing to the irregularity and wide size distribution of COF. The organic monolithic column is superb in permeability and mass transfer but poor in column efficiency for small molecules due to the lack of interaction sites.[20,21] The integration of 3D COF and a porous monolith is an efficient method to solve the above-mentioned limitations of the two materials. The porous organic monolith ensures the permeability of the prepared 3D COF column, while the well-ordered structure of 3D COF brings the monolith diverse interactions with various small molecules.[22,23] However, to our knowledge, no study on the preparation and application of a 3D COF monolithic column for HPLC has been reported so far.

Received: March 19, 2021
Accepted: April 14, 2021
Published: April 23, 2021

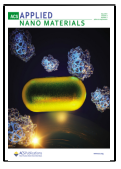

https://doi.org/10.1021/acsanm.1c00770
ACS Appl. Nano Mater. 2021, 4, 5437−5443

Scheme 1. Preparation of a 3D-IL-COF-1 Monolithic Column for HPLC

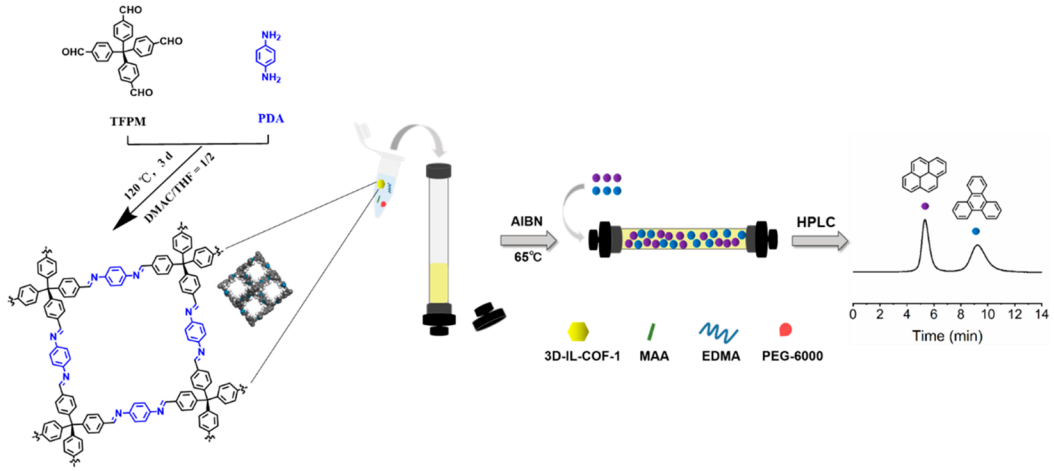

Herein, we report the first synthesis of a 3D COF-incorporated monolithic column for HPLC. The model 3D COF 3D-IL-COF-1 with a nanoporous 5-fold interpenetrated dia net structure was prepared with tetrakis(4-formylphenyl)-methane (TFPM) and *p*-phenylenediamine (PDA) via the typical solvothermal method instead of the reported ionothermal synthesis and was incorporated into methylacrylic acid-*co*-ethylene dimethacrylate (MAA-*co*-EDMA) monolith to obtain the 3D-IL-COF-1 monolithic column. An orthogonal experiment was designed to investigate the effect of essential factors including temperature, porogen, and 3D-IL-COF-1 on the column permeability and efficiency. The chromatographic performance of the 3D-IL-COF-1 monolithic column was demonstrated with typical neutral, acidic, and basic compounds as well as isomers.

EXPERIMENTAL SECTION

Orthogonal Design for the Preparation of a 3D-IL-COF-1 Monolithic Column. The levels of three factors (temperature, porogen, and 3D COF) for the synthesis of the 3D-IL-COF-1 monolithic column were determined with single-factor experiments. Then, a $L_9(3^3)$ array was designed to assign the obtained levels of temperature, porogen, and 3D COF for the orthogonal investigation of the preparation of the 3D-IL-COF-1 monolithic column.

Synthesis of a 3D-IL-COF-1 Monolithic Column. Typically, 3D-IL-COF-1 (15 mg), MAA (35 μL), EDMA (400 μL), and polyethylene glycol 6000 (PEG-6000) (450 mg) were dissolved in dimethyl sulfoxide (DMSO) (1 mL) to obtain a stable and uniform dispersion, and then 2,2-azobis(2-methylpropionitrile) (AIBN) (10 mg) was added. The resulting mixture was moved into a stainless-steel column (50.0 mm long × 4.6 mm i.d.). After sealing, the column was left in a thermostat water bath at 65 °C for 24 h and then rinsed with acetylene (ACN) to clear up the residual reactant and porogen to obtain the 3D-IL-COF-1 monolithic column. The blank monolithic column as a control was subject to the same conditions without the addition of 3D-IL-COF-1.

HPLC Experiments. The 3D-IL-COF-1 monolithic column must be conditioned with the corresponding mobile phase prior to the HPLC experiment. All of the HPLC experiments were carried out on an e2695 liquid chromatograph (Waters, USA) with a 2998 tunable photodiode array detector. Collection and analysis of the chromatographic data was performed on an Empower data system. The C18 column (50.0 mm long × 4.6 mm i.d.) for comparison of the 3D-IL-COF-1 monolithic column was prepared with commercial C18 spherical silica (Baseline ChromTech Research Centre, Tianjin, China).

RESULTS AND DISCUSSION

Preparation of a 3D-IL-COF-1 Monolithic Column. Direct packaging of the 3D-IL-COF-1 as the stationary phase in stainless-steel column (50.0 mm long × 4.6 mm i.d.) for HPLC was not successful due to the irregular morphology and wide size distribution of 3D-IL-COF-1. Integration of 3D COF and the porous monolith is a promising way to solve the limitation and is of great significance for expanding their high potential in HPLC. However, no study on the preparation and application of a 3D COF monolithic column for HPLC has been reported so far. Scheme 1 shows the method for the preparation of the 3D-IL-COF-1 monolithic column for HPLC. 3D-IL-COF-1 was first prepared from TFPM and PDA via the typical solvothermal method due to the benefit to yields instead of the reported ionothermal synthesis.[1,13] The 3D-IL-COF-1 monolithic column was then fabricated by incorporating 3D-IL-COF-1 into a poly(MAA-*co*-EDMA) monolith.

The single-factor experiments for the effect of polymerization temperature, porogen, and 3D-IL-COF-1 on the preparation of the monolithic column were investigated in the range of 55−75 °C, 300−500 mg, and 5−20 mg, respectively (Figure S1). The increase of temperature improved the efficiency but decreased the permeability of the 3D-IL-COF-1 monolithic column (Figure S1A). The high temperature gives a large number of free radicals and formulates more small pores in the monolith, which is favorable for column efficiency but detrimental to permeability.[24−26] On the contrary, amplification of the porogen leads to the amelioration of the column permeability but loss of column efficiency. The porogen is produced through pores in the 3D-IL-COF-1 monolith to promote the permeability, but too many pores went against the column efficiency (Figure S1B). A 15 and 20 mg amount of 3D-IL-COF-1 gave better column permeability and efficiency, respectively. Further increasing the amount of 3D-IL-COF-1 resulted in a decrease of both the column permeability and the efficiency (Figure S1C). Three levels of temperature (60, 65, and 70 °C), porogen (350, 400, and 450 mg), and 3D-IL-COF-1 (10, 15, and 20 mg) were then selected for further orthogonal design to obtain the optimal synthetic conditions for both the column permeability and the efficiency.

The orthogonal experiment significantly reduces the number of experiments and scientifically analyzes the data.[26−28] A

https://doi.org/10.1021/acsanm.1c00770
ACS Appl. Nano Mater. 2021, 4, 5437−5443

Table 1. Range Analysis of the $L_9(3^3)$ Array Results for the Orthogonal Design Experiment[a]

	colum permeability ($\times 10^{-15}$ m^2)			column efficiency ($\times 10^3$ plates m^{-1})		
parameters	temperature	porogen	3D COF	temperature	porogen	3D COF
*K*1	18.14	15.35	17.77	15.30	17.07	10.63
*K*2	18.86	18.74	19.19	19.03	16.94	19.91
*K*3	19.11	22.02	19.15	16.36	16.68	20.15
R	0.97	6.67	1.42	3.73	0.39	9.53

[a]The *K* is the average experimental results of each factor level for column permeability or efficiency. The *R* is the difference between the minimum and the maximum of *K* for column permeability or efficiency.

Table 2. Variance Analysis of the $L_9(3^3)$ Array Results for the Orthogonal Design Experiment[a]

	column permeability			column efficiency		
parameters	temperature	porogen	3D COF	temperature	porogen	3D COF
$SS \times 10^{-30}$	1.51	66.81	3.94	33.02	7.94	152.38
df	2	2	2	2	2	2
$MS \times 10^6$	0.76	33.40	1.97	16.51	3.97	76.19
F	2.65	116.79	6.89	22.85	5.50	105.45
P	0.274	0.008[c]	0.127	0.042[b]	0.154	0.009[c]

[a]*SS* (squares of deviation), *df* (degree of freedom), and *MS* (mean squared deviation). $F_{0.05}(2,2) = 19.00$, $F_{0.01}(2,2) = 99.01$. [b]$0.01 < p \leq 0.05$, [c]$p \leq 0.01$

$L_9(3^3)$ orthogonal array assigned with temperature, porogen, and 3D-IL-COF-1 in three levels was designed to investigate the preparation of the 3D-IL-COF-1 monolithic column (Tables S1 and S2). The *R* value in range analysis represents the effect of factors on the experimental results.[28−31] The *R* value for column permeability ($R_{porogen} > R_{3D\text{-}IL\text{-}COF\text{-}1} > R_{temperature}$) and column efficiency ($r_{3D\text{-}IL\text{-}COF\text{-}1} > r_{temperature} > r_{porogen}$) indicates the highest effect of porogen and 3D-IL-COF-1 on the permeability and column efficiency, respectively (Table 1). Furthermore, the *P* value in variance analysis reveals the significance of factors on the experimental results.[28,31] The porogen had an extremely significant influence on the permeability. A 450 mg amount of porogen with the best permeability (*K*3) was employed for preparation of the 3D-IL-COF-1 monolithic column (Table 2). Both 3D-IL-COF-1 and temperature had a significant influence on the column efficiency. Both 65 °C and a 15 mg amount of 3D-IL-COF-1 with the highest column efficiency (*K*2) were finally selected for further preparation of the 3D-IL-COF-1 monolithic column.

Characterization of 3D-IL-COF-1 and Its Monolith. The main characteristic powder X-ray diffraction (PXRD) peaks of the obtained COF at 7.36°, 9.63°, 13.27°, 14.93°, and 16.50° matched well with the simulated one, indicating the preparation of crystalline 3D-IL-COF-1 (Figure 1A). The 3D-IL-COF-1 kept its main PXRD pattern under the same preparation procedure for the 3D-IL-COF-1 monolithic column without the addition of cross-linking agent (MAA and EDMA), indicating the maintenance of the crystallinity for 3D-IL-COF-1 in the 3D-IL-COF-1 monolith (Figure S2). Furthermore, no change in the PXRD pattern and Fourier transform infrared spectroscopy (FT-IR) spectra of 3D-IL-COF-1 in DMSO, ACN, and H_2O suggests the high stability of the COF (Figure S3). The appearance of the characteristic imine band at 1618 cm^{-1} along with the evident attenuation of the aldehyde (1700 cm^{-1}) and amino (3200−3500 cm^{-1}) bands of the original building monomers in the FT-IR spectra suggest the successful condensation of TFPM and PDA (Figure S4). The FT-IR spectra of the 3D-IL-COF-1 monolith displayed the three characteristic bands (1727, 1259, and 1158 cm^{-1}) of poly(MAA-*co*-EDMA) as well as those (1569, 1017, and 829 cm^{-1}) of 3D-IL-COF-1 (Figure 1B), suggesting the successful incorporation of 3D COF. The scanning and transmission electron microscopy images reveal the typical spherical morphology of 3D-IL-COF-1 (Figure S5). The 3D-IL-COF-1 monolith showed a porous monolithic structure with interconnected pores (Figure S6). The prepared 3D-IL-COF-1 monolith had a significantly larger BET surface area

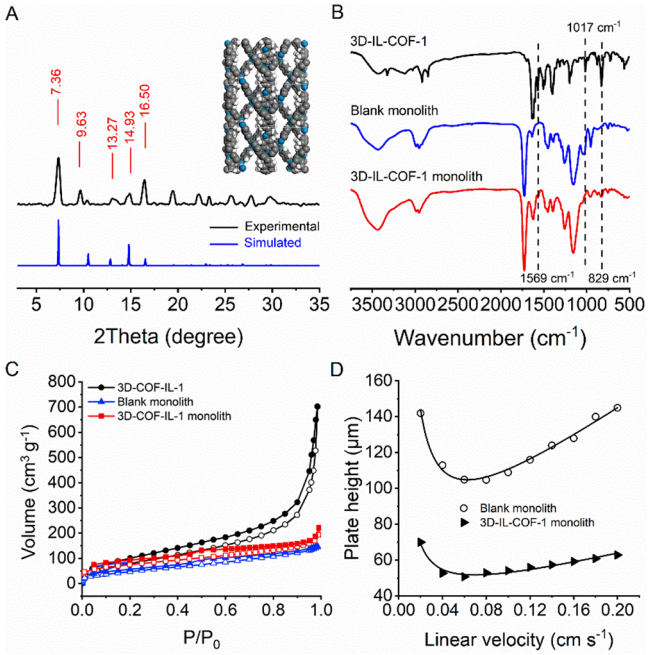

Figure 1. (A) PXRD pattern of the prepared 3D-IL-COF-1. (Insert) Graphic view of 3D-IL-COF-1 (C, gray; N, blue; O, white). (B) FT-IR spectra and (C) N_2 adsorption−desorption isotherms of 3D-IL-COF-1, blank monolith, and 3D-IL-COF-1 monolith. (D) Van Deemter plots of 3D-IL-COF-1 and blank monolithic column with toluene as analyte. Mobile phase and flow rate: ACN/H_2O (70/30, v/v) at 0.2−5 mL min^{-1}; UV wavelength at 210 nm; temperature, 25 °C.

https://doi.org/10.1021/acsanm.1c00770
ACS Appl. Nano Mater. 2021, 4, 5437−5443

(251 m^2 g^{-1}) than the blank monolith (186 m^2 g^{-1}) owing to the incorporation of a larger BET surface area of 3D-IL-COF-1 (934 m^2 g^{-1}) (Figure 1C and Figure S7).

Assessment of 3D-IL-COF-1 Monolithic Column. The fabricated 3D-IL-COF-1 monolithic column was first evaluated using the Van Deemter model.[32] The highest theoretical plate number of toluene (model analyte) on the 3D-IL-COF-1 monolithic column was investigated using ACN/H_2O (70/30, v/v) in the flow rate range of 0.2−2 mL min^{-1} (Figure 1D). The 3D-IL-COF-1 monolithic column offered a significant improvement in the highest theoretical plate number (20 700 plates m^{-1}) compared to the blank monolithic column (9541 plates m^{-1}), implying the distinctive role of the incorporated 3D-IL-COF-1. The vortex diffusion (A), longitudinal diffusion (B), and mass resistance (C) terms of the Van Deemter curve for the 3D-IL-COF-1 monolithic column were significantly lower than those of the blank monolithic column (Table S3). A reduction of the A value indicates more uniformity of the 3D-IL-COF-1 monolith than the blank monolith. The decrease of the B and C values represents less diffusion of the solute in the mobile phase and faster mass transmission between the 3D-IL-COF-1 monolith and the analytes, resepectively.[33,34] The above results convey the significant role of the 3D-IL-COF-1 in the improvement of the separation efficiency on the monolithic column.

The effect of the flow rate on the pressure of the 3D-IL-COF-1 monolithic column was studied in the flow rate range of 0.2−5 mL min^{-1} using ACN, ACN/H_2O (50/50, v/v), methanol (MeOH), and MeOH/H_2O (50/50, v/v) as the mobile phase. An excellent linear relationship was obtained for all four mobile phases in the studied flow rate range (R^2, 0.9961−0.9998) (Figure S8). No structure collapse appeared in the 3D-IL-COF-1 monolithic column even at column pressures up to 2170 psi with MeOH/H_2O (50/50, v/v) at a flow rate of 5 mL min^{-1}. The proved great mechanical stability of 3D-IL-COF-1 shows the potential of the as-prepared 3D-IL-COF-1 monolithic column in rapid HPLC separation with diverse mobile phases.

HPLC Separation of Neutral, Acidic, and Basic Compounds. The broad-spectrum chromatography performance of the 3D-IL-COF-1 monolithic column was evaluated by the separation of neutral, acidic, and basic compounds. The 3D-IL-COF-1 monolithic column gave baseline separation of neutral alkylbenzenes (benzene, toluene, ethylbenzene, propylene, and butylbenzene) and polycyclic aromatic hydrocarbons (PAHs) (benzene, naphthalene, anthracene, pyrene, and benzopyrene) (Figure 2A and 2B). The elution orders of the alkylbenzenes and PAHs on the 3D-IL-COF-1 monolith were in good agreement with those on a C18 column (Figure S9), indicating the main hydrophobic interaction during the separation.[35,36] The strong retention of the PAHs on the 3D-IL-COF-1 monolithic column also revealed the involvement of a $\pi-\pi$ interaction in the separation of the PAHs (Figure 2B).[35,36] The increasing ACN content led to a decrease of retention, resolution (R), and column efficiency (Figure S10, Tables S4 and S5), confirming the typical reverse phase separation mechanism of the 3D-IL-COF-1 monolithic column for alkylbenzenes and PAHs.[37,38]

The baseline separation of the acidic phenol compounds (*m*-nitrophenol, 2,6-dimethylphenol, and 2,6-dichlorophenol) and basic aniline compounds (aniline, *m*-nitroaniline, and *N*,*N*-dimethylaniline) was also realized on the 3D-IL-COF-1 monolithic column (Figure 2C and 2D). The elution

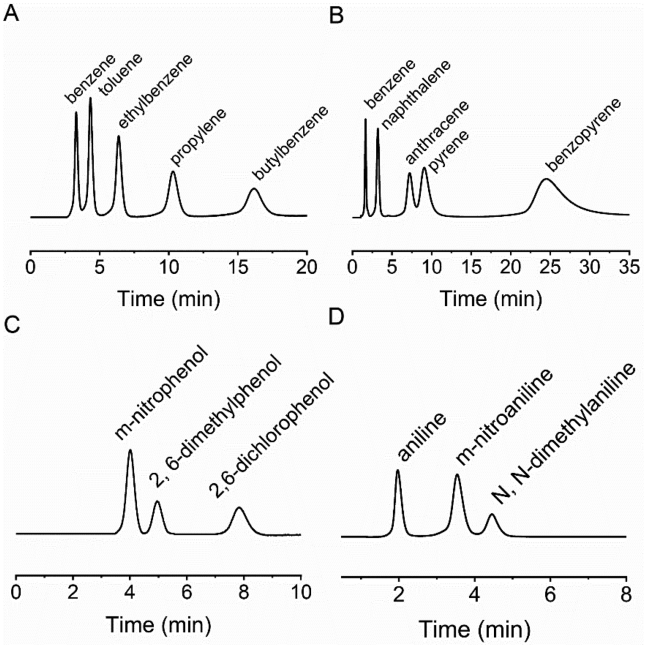

Figure 2. HPLC chromatograms of neutral, acidic, and basic compounds on a 3D-IL-COF-1 monolithic column (50.0 mm × 4.6 mm i.d.): (A) alkylbenzenes; (B) PAHs; (C) acidic compounds; (D) basic compounds. Mobile phase and flow rate: ACN/H_2O (35/65, v/v) at 1.0 mL min^{-1} for A and D, ACN/H_2O (45/55, v/v) at 1.0 mL min^{-1} for B, and ACN/H_2O (30/70, v/v) at 1.0 mL min^{-1} for C. UV wavelength at 210 nm. Temperature, 25 °C.

sequences of all of the analytes were consistent with their hydrophobicity (Table S6), demonstrating that hydrophobic interaction played a key role in the separation. The selectivity factor (k) and R of the six analytes on the 3D-IL-COF-1 monolithic column were comparable with those on a C18 column (Tables S7 and S8). The blank monolithic column without 3D-IL-COF-1 gave no separation of the above neutral, acidic, and basic compounds (Figure S11), proving the dominant of 3D-IL-COF-1 in the chromatography separation.

HPLC Separation of Isomers. The similar properties of the isomers lead to a great challenge in their separation.[39] The performance of the 3D-IL-COF-1 monolithic column was further investigated for separation of isomers including *o*-, *m*-, and *p*-aminophenol, acenaphthene and fluorene, phenanthrene and anthracene, and pyrene and triphenylene (Figure 3). The 3D-IL-COF-1 monolithic column gave better separation for these isomers than the blank monolithic column and the C18 column. The blank monolithic column showed no separation of all of the isomers (Figure S12). The C18 column enabled the separation of phenanthrene and anthracene and pyrene and triphenylene but gave no baseline separation of *o*-, *m*-, and *p*-aminophenol and fluorene and acenaphthene (Figure S13). Moreover, the 3D-IL-COF-1 monolithic column gave a higher k (1.23−1.75) than the C18 column (1.06−1.32) for all of the studied analytes (Tables S9 and S10), indicating the great potential of the 3D-IL-COF-1 monolithic column in isomer separation.

We further investigated the separation mechanism of the isomers on the 3D-IL-COF-1 monolithic column. The smaller molecular size of *o*-, *m*-, and *p*-aminophenol than the pore size of 3D-IL-COF-1 (8.4 Å) indicates the interaction of aminophenol isomers in the inner pore of the COF. The octanol−water partition coefficient (K_{ow}) is usually used to

https://doi.org/10.1021/acsanm.1c00770
ACS Appl. Nano Mater. 2021, 4, 5437−5443

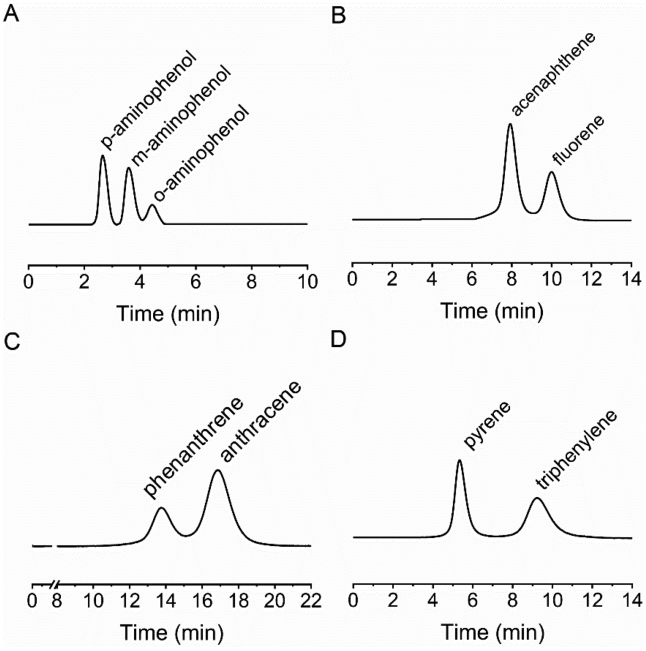

Figure 3. HPLC separation of isomers on a 3D-IL-COF-1 monolithic column (50.0 mm × 4.6 mm i.d.): (A) *o*-, *m*-, and *p*-aminophenol; (B) acenaphthene and fluorene; (C) phenanthrene and anthracene; (D) pyrene and triphenylene. Mobile phase and flow rate: ACN/H_2O (25/75, v/v) at 1.0 mL min^{-1} for A, ACN/H_2O (40/60, v/v) at 1.4 mL min^{-1} for B and C, and ACN/H_2O (55/45, v/v) at 1.2 mL min^{-1} for D. Temperature, 25 °C. UV wavelength at 210 nm for A, B, and D and 254 nm for C.

indicate the hydrophobicity of organic compounds. The identical hydrophobicity of *o*-, *m*-, and *p*-aminophenol (log K_{ow} 0.62) means that the hydrophobic interaction cannot drive their separation. The different hydrogen bonding ability of the aminophenol isomers should be responsible for their separation. The weakest acidity of *p*-aminophenol (pK_a 5.48) resulted in the weakest hydrogen bonding with 3D-IL-COF-1 monolith and made it elute first. The closer hydroxyl and amino groups of *o*-aminophenol enabled simultaneous formation of a hydrogen bond with 3D-IL-COF-1 and showed a stronger retention than *m*-aminophenol. The apparent difference in the hydrophobicity of acenaphthene and fluorene or pyrene and triphenylene revealed the dominant hydrophobic interaction in their separation. In contrast, the elution order of phenanthrene and anthracene did not follow their hydrophobicity (Table S11). Although the PAHs isomers cannot completely enter the pore of 3D-IL-COF-1 (Table S11), the "slot model" shows that the larger length-to-breadth ratio (L/B) of PAHs can penetrate to a greater depth in the slot.[40,41] Hence, the larger L/B of anthracene (1.57) gave it easier access to the 3D-IL-COF-1 monolith and so stronger retention than phenanthrene (L/B, 1.46).[42,43]

The good linearity of the Van't Hoff plots for isomers on the 3D-IL-COF-1 monolith implies that the separation mechanism has little change within the studied temperature range[15] (Figure S14). The thermodynamic parameters for the separation of isomers on the 3D-IL-COF-1 monolithic column were further calculated from Van't Hoff plots (Table. S12). The negative enthalpy change (ΔH) shows that the separation behavior of the isomers on the 3D-IL-COF-1 monolithic column is exothermic. The negative Gibbs free energy change (ΔG) indicates that the transference of all of the analytes from the mobile phase to the stationary phase of 3D-IL-COF-1 is a thermodynamically spontaneous process.

Repeatability and Stability of a 3D-IL-COF-1 Monolithic Column. The relative standard deviations (RSDs) of retention time (t_R) and peak area (S) for pyrene and triphenylene in 10 continuous injections (run to run, n = 10) were 0.27−0.50% and 1.28−1.40%, respectively (Figure S15, Table. S13). The five continuous days analysis (day to day, n = 5) of the analytes gave RSDs of 0.81−1.04% and 2.20−2.93% for t_R and S, respectively. Moreover, the three columns obtained from different batches (column to column, n = 3) still gave low RSDs of t_R (1.11−1.90%) and S (3.21−4.64%). The results showed the great repeatability and stability of the 3D-IL-COF-1 monolithic column for HPLC separation.

CONCLUSION

In summary, we have shown the synthesis of the first 3D COF-based monolithic column via the facile incorporation of nanoporous 3D-IL-COF-1 into a porous organic monolith for HPLC. The porous organic monolith matrix ensures the permeability of the prepared 3D COF monolithic column, and the introduction of 3D-IL-COF-1 provided the monolithic column with various interactions for promotion of its HPLC application. The uniform structure, good permeability, and high mechanical stability of the prepared 3D-IL-COF-1 monolithic column not only make it promising for broad-spectrum chromatographic separation of neutral, acidic, and basic compounds but also render it better separation of isomers than a C18 column. We believe this work will largely expand 3D COF as stationary phase for HPLC.

ASSOCIATED CONTENT

Supporting Information

The Supporting Information is available free of charge at https://pubs.acs.org/doi/10.1021/acsanm.1c00770.

Additional information including general method, apparatus, and supplementary figures and tables as mentioned in the text (PDF)

AUTHOR INFORMATION

Corresponding Authors

Hai-Long Qian − *International Joint Laboratory on Food Safety and Institute of Analytical Food Safety, School of Food Science and Technology, Jiangnan University, Wuxi 214122, China;* orcid.org/0000-0001-7554-4115; Email: hlqian@jiangnan.edu.cn

Xiu-Ping Yan − *State Key Laboratory of Food Science and Technology, International Joint Laboratory on Food Safety, Institute of Analytical Food Safety, School of Food Science and Technology, and Key Laboratory of Synthetic and Biological Colloids, Ministry of Education, Jiangnan University, Wuxi 214122, China;* orcid.org/0000-0001-9953-7681; Email: xpyan@jiangnan.edu.cn

Authors

Xue Liu − *Institute of Analytical Food Safety, School of Food Science and Technology, Jiangnan University, Wuxi 214122, China*

Cheng Yang − *International Joint Laboratory on Food Safety and Institute of Analytical Food Safety, School of Food Science and Technology, Jiangnan University, Wuxi 214122, China*

https://doi.org/10.1021/acsanm.1c00770
ACS Appl. Nano Mater. 2021, 4, 5437−5443

Complete contact information is available at:
https://pubs.acs.org/10.1021/acsanm.1c00770

Notes

The authors declare no competing financial interest.

■ ACKNOWLEDGMENTS

We are thankful for the support of the National Natural Science Foundation of China (Nos. 21804055, 21775056, 22076066), the Natural Science Foundation of Jiangsu Province (No. BK20180585), the Fundamental Research Funds for the Central Universities (No. JUSRP221002), the National First-Class Discipline Program of Food Science and Technology (No. JUFSTR20180301), and the Program of the "Collaborative Innovation Center of Food Safety and Quality Control in Jiangsu Province".

■ REFERENCES

(1) Feng, X.; Ding, X.; Jiang, D. Covalent Organic Frameworks. *Chem. Soc. Rev.* **2012**, *41*, 6010−6022.
(2) Yuan, F.; Tan, J.; Guo, J. Assemblies of Covalent Organic Framework Microcrystals: Multiple-Dimensional Manipulation for Enhanced Applications. *Sci. China: Chem.* **2018**, *61*, 143−152.
(3) Qian, H. L.; Meng, F. L.; Yang, C. X.; Yan, X. P. Irreversible Amide-Linked Covalent Organic Framework for Selective and Ultrafast Gold Recovery. *Angew. Chem. Int. Ed.* **2020**, *59*, 17607−17613.
(4) Das, S.; Feng, J.; Wang, W. Covalent Organic Frameworks in Separation. *Annu. Rev. Chem. Biomol. Eng.* **2020**, *11*, 131−153.
(5) Salonen, L. M.; Pinela, S. R.; Fernandes, S. P. S.; Loucano, J.; Carbo-Argibay, E.; Sarria, M. P.; Rodriguez-Abreu, C.; Peixoto, J.; Espina, B. Adsorption of Marine Phycotoxin Okadaic Acid on a Covalent Organic Framework. *J. Chromatogr. A* **2017**, *1525*, 17−22.
(6) Liu, J. M.; Wang, X. Z.; Zhao, C. Y.; Hao, J. L.; Fang, G. Z.; Wang, S. Fabrication of Porous Covalent Organic Frameworks as Selective and Advanced Adsorbents for the On-Line Preconcentration of Trace Elements Against the Complex Sample Matrix. *J. Hazard. Mater.* **2018**, *344*, 220−229.
(7) Wang, J.; Zhuang, S. Covalent Organic Frameworks (COFs) for Environmental Applications. *Coord. Chem. Rev.* **2019**, *400*, 213046−213062.
(8) Liu, X.; Huang, D.; Lai, C.; Zeng, G.; Qin, L.; Wang, H.; Yi, H.; Li, B.; Liu, S.; Zhang, M.; Deng, R.; Fu, Y.; Li, L.; Xue, W.; Chen, S. Recent Advances in Covalent Organic Frameworks (COFs) as a Smart Sensing Material. *Chem. Soc. Rev.* **2019**, *48*, 5266−5302.
(9) Guan, Q.; Zhou, L. L.; Li, W. Y.; Li, Y. A.; Dong, Y. B. Covalent Organic Frameworks (COFs) for Cancer Therapeutics. *Chem. - Eur. J.* **2020**, *26*, 5583−5591.
(10) Saha, S.; Walia, S.; Sharma, K.; Banerjee, K. Suitability of Stationary Phase for LC Analysis of Biomolecules. *Crit. Rev. Food Sci. Nutr.* **2020**, *60*, 2856−2873.
(11) Zuvela, P.; Skoczylas, M.; Jay Liu, J.; Baczek, T.; Kaliszan, R.; Wong, M. W.; Buszewski, B. Column Characterization and Selection Systems in Reversed-Phase High-Performance Liquid Chromatography. *Chem. Rev.* **2019**, *119*, 3674−3729.
(12) Huang, X.; Sun, C.; Feng, X. Crystallinity and Stability of Covalent Organic Frameworks. *Sci. China: Chem.* **2020**, *63*, 1367−1390.
(13) Guan, X.; Ma, Y.; Li, H.; Yusran, Y.; Xue, M.; Fang, Q.; Yan, Y.; Valtchev, V.; Qiu, S. Fast, Ambient Temperature and Pressure Ionothermal Synthesis of Three-Dimensional Covalent Organic Frameworks. *J. Am. Chem. Soc.* **2018**, *140*, 4494−4498.
(14) Ma, X.; Scott, T. F. Approaches and Challenges in the Synthesis of Three-Dimensional Covalent-Organic Frameworks. *Commun. Chem.* **2018**, *1*, 98−112.
(15) Liu, L. H.; Yang, C. X.; Yan, X. P. Methacrylate-Bonded Covalent-Organic Framework Monolithic Columns for High Performance Liquid Chromatography. *J. Chromatogr. A* **2017**, *1479*, 137−144.
(16) Yang, C. X.; Liu, C.; Cao, Y. M.; Yan, X. P. Facile Room-Temperature Solution-Phase Synthesis of a Spherical Covalent Organic Framework for High-Resolution Chromatographic Separation. *Chem. Commun.* **2015**, *51*, 12254−12257.
(17) Zhang, K.; Cai, S. L.; Yan, Y. L.; He, Z. H.; Lin, H. M.; Huang, X. L.; Zheng, S. R.; Fan, J.; Zhang, W. G. Construction of a Hydrazone-Linked Chiral Covalent Organic Framework-Silica Composite as the Stationary Phase for High Performance Liquid Chromatography. *J. Chromatogr. A* **2017**, *1519*, 100−109.
(18) Zuo, H.; Guo, Y.; Zhao, W.; Hu, K.; Wang, X.; He, L.; Zhang, S. Controlled Fabrication of Silica@Covalent Triazine Polymer Core-Shell Spheres as a Reversed-Phase/Hydrophilic Interaction Mixed-Mode Chromatographic Stationary Phase. *ACS Appl. Mater. Interfaces* **2019**, *11*, 46149−46156.
(19) Huang, J.; Han, X.; Yang, S.; Cao, Y.; Yuan, C.; Liu, Y.; Wang, J.; Cui, Y. Microporous 3D Covalent Organic Frameworks for Liquid Chromatographic Separation of Xylene Isomers and Ethylbenzene. *J. Am. Chem. Soc.* **2019**, *141*, 8996−9003.
(20) Nischang, I.; Teasdale, I.; Brüggemann, O. Porous Polymer Monoliths for Small Molecule Separations: Advancements and Limitations. *Anal. Bioanal. Chem.* **2011**, *400*, 2289−2304.
(21) Tanaka, N.; Kobayashi, H.; Ishizuka, N.; Minakuchi, H.; Nakanishi, K.; Hosoya, K.; Ikegami, T. Monolithic Silica Columns for High-Efficiency Chromatographic Separations. *J. Chromatogr. A* **2002**, *965*, 35−49.
(22) Guan, X.; Chen, F.; Fang, Q.; Qiu, S. Design and Applications of Three Dimensional Covalent Organic Frameworks. *Chem. Soc. Rev.* **2020**, *49*, 1357−1384.
(23) El-Kaderi, H. M.; Hunt, J. R.; Mendoza-Cortes, J. L.; Cote, A. P.; Taylor, R. E.; O'Keeffe, M.; Yaghi, O. M. Designed Synthesis of 3D Covalent Organic Frameworks. *Science* **2007**, *316*, 268−272.
(24) Viklund, C.; Svec, F.; Frechet, J. M. J.; Irgum, K. Monolithic, "Molded", Porous Materials with High Flow Characteristics for Separations, Catalysis, or Solid-Phase Chemistry: Control of Porous Properties during Polymerization. *Chem. Mater.* **1996**, *8*, 744−750.
(25) Svec, F. Porous Polymer Monoliths: Amazingly Wide Variety of Techniques Enabling their Preparation. *J. Chromatogr. A* **2010**, *1217*, 902−924.
(26) Svec, F.; Frechet, J. M. J. Temperature, a Simple and Efficient Tool for the Control of Pore Size Distribution in Macroporous Polymers. *Macromolecules* **1995**, *28*, 7580−7582.
(27) Huynh, T. V. Orthogonal Array Experiment in Systems Engineering and Architecting. *Syst. Eng.* **2011**, *14*, 208−222.
(28) Yuan, Z.; Chen, X.; Zeng, H.; Wang, K.; Qiu, J. Identification of the Elastic Constant Values for Numerical Simulation of High Velocity Impact on Dyneema Woven Fabrics Using Orthogonal Experiments. *Compos. Struct.* **2018**, *204*, 178−191.
(29) Wu, X.; Leung, D. Y. C. Optimization of Biodiesel Production from Camelina Oil Using Orthogonal Experiment. *Appl. Energy* **2011**, *88*, 3615−3624.
(30) Zhou, L.; Shi, W.; Wu, S. Performance Optimization in a Centrifugal Pump Impeller by Orthogonal Experiment and Numerical Simulation. *Adv. Mech. Eng.* **2013**, *5*, 385809−385815.
(31) Chuanwen, C.; Feng, S.; Yuguo, L.; Shuyun, W. Orthogonal Analysis for Perovskite Structure Microwave Dielectric Ceramic Thin Films Fabricated by the RF Magnetron-Sputtering Method. *J. Mater. Sci.: Mater. Electron.* **2010**, *21*, 349−354.
(32) Van Deemter, J. J.; Zuiderweg, F. J.; Klinkenberg, A. Longitudinal Diffusion and Resistance to Mass Transfer as Causes of Nonideality in Chromatography. *Chem. Eng. Sci.* **1956**, *5*, 271−289.
(33) Asiaie, R.; Huang, X.; Farnan, D.; Horváth, C. Sintered Octadecylsilica as Monolithic Column Packing in Capillary Electrochromatography and Micro High-Performance Liquid Chromatography. *J. Chromatogr. A* **1998**, *806*, 251−263.
(34) Yan, L. J.; Zhang, Q. H.; Feng, Y. Q.; Zhang, W. B.; Li, T.; Zhang, L. H.; Zhang, Y. K. Octyl-Functionalized Hybrid Silica

Monolithic Column for Reversed-Phase Capillary Electrochromatography. *J. Chromatogr. A* **2006**, *1121*, 92−98.
(35) Xi, Y.; Du, Y.; Sun, X.; Zhao, S.; Feng, Z.; Chen, C.; Ding, W. A Monolithic Capillary Modified with a Copoplymer Prepared from the Ionic Liquid 1-Vinyl-3-Octylimidazolium Bromide and Styrene for Electrochromatography of Alkylbenzenes, Polycyclic Aromatic Hydrocarbons, Proteins and Amino Acids. *Microchim. Acta* **2020**, *187*, 67−74.
(36) Chen, L.; Gao, J.; Wu, Q.; Li, H.; Dong, S.; Shi, X.; Zhao, L. Preparation and Performance of a Novel Multi-Mode COF-300@ SiO_2 Chromatographic Stationary Phase. *Eur. Polym. J.* **2019**, *116*, 9−19.
(37) Li, X.; Li, B.; Liu, M.; Zhou, Y.; Zhang, L.; Qiao, X. Core-Shell Metal-Organic Frameworks as the Mixed-Mode Stationary Phase for Hydrophilic Interaction/Reversed-Phase Chromatography. *ACS Appl. Mater. Interfaces* **2019**, *11*, 10320−10327.
(38) Wang, S.; Zhang, L.; Xiao, R.; Chen, H.; Chu, Z.; Zhang, W.; Liu, F. Fabrication of SiO_2@COF5 Microspheres and their Application in High Performance Liquid Chromatography. *Anal. Methods* **2018**, *10*, 1968−1976.
(39) Qian, H. L.; Yang, C.; Yan, X. P. Layer-by-layer Preparation of 3D Covalent Organic Framework/Silica Composites for Chromatographic Separation of Position Isomers. *Chem. Commun.* **2018**, *54*, 11765−11768.
(40) Wise, S. A.; Sander, L. C. Factors Affecting the Reversed-Phase Liquid Chromatographic Separation of Polycyclic Aromatic Hydrocarbon Isomers. *J. High Resolut. Chromatogr.* **1985**, *8*, 248−255.
(41) Wise, S. A.; Sander, L. C.; Lapouyade, R.; Garrigues, P. Anomalous Behavior of Selected Methyl-Substituted Polycyclic Aromatic Hydrocarbons in Reversed-Phase Liquid Chromatography. *J. Chromatogr. A* **1990**, *514*, 111−122.
(42) Oña-Ruales, J. O.; Sander, L. C.; Wilson, W. B.; Wise, S. A. Revisiting Shape Selectivity in Liquid Chromatography for Polycyclic Aromatic Hydrocarbons (PAHs) − Six-Ring and Seven-Ring Cata-Condensed PAH Isomers of Molecular Mass 328 and 378 Da. *Anal. Bioanal. Chem.* **2018**, *410*, 885−896.
(43) Lippa, K. A.; Sander, L. C.; Wise, S. A. Chemometric Studies of Polycyclic Aromatic Hydrocarbon Shape Selectivity in Reversed-Phase Liquid Chromatography. *Anal. Bioanal. Chem.* **2004**, *378*, 365−377.

https://doi.org/10.1021/acsanm.1c00770
ACS Appl. Nano Mater. 2021, 4, 5437−5443